Thermal Properties and Three-Phase Structure of *cis*-1,4-Polybutadiene

Maria Laura Di Lorenzo*

Istituto di Chimica e Tecnologia dei Polimeri (CNR) – c/o Comprensorio Olivetti – Via Campi Flegrei, 34 – 80078 Pozzuoli (NA), Italy

Abstract: The thermal properties of *cis*-1,4-polybutadiene (*cis*-PBD) were investigated in dependence of content of *cis* units and of linearity of the main chain. *cis*-PBD grades containing a fraction of *cis*-segments ranging from 93 to 98 %, and with linear or branched chains, were analyzed. Upon isothermal crystallization from the melt at -26 °C for 1 h, followed by cooling to below the glass transition temperature, *cis*-PBD develops a three-phase structure, where the mobile amorphous phase is equal to 0.41, independently of chain structure, crystallinity ranges from 0.23 to 0.28, and the rigid amorphous fraction varies from 0.31 to 0.35. Up to three main endotherms can be evidenced by calorimetry at slow heating rate, depending on chain regularity. The multiple melting behavior was discussed on the basis of the three-phase structure, as well as of crystallization kinetics.

Keywords: *cis*-1,4-polybutadiene, calorimetry, multiple melting, crystallization, rigid amorphous fraction.

INTRODUCTION

Polybutadiene with a large content of *cis*-1,4-units (*cis*-PBD) is one of the most common polymers produced by the modern synthetic rubber industry, being it widely used for the production of tires [1]. Polybutadiene also has a major application for the production of golf balls, as well as impact modifier for polystyrene and acrylonitrile-butadiene-styrene resin (ABS) [1].

Cis-1,4-polybutadiene is a semicrystalline polymer. Semicrystalline polymers are often described in terms of a two-phase structure, composed of amorphous and crystalline moieties, where the sum of the mass fraction of the amorphous (w_A) and the crystalline (w_C) parts is equal to 1:

$$w_C + w_A = 1 \quad (1)$$

However, polymer science literature suggests that the above equation is often incorrect, as it is now recognized that a fraction of the amorphous material in semi-crystalline polymers has a restrained molecular mobility. This portion, that does not contribute to the bulk glass transition, is known as "rigid amorphous fraction" (RAF) and seems to be located at the interface between the crystalline and the mobile amorphous phases [2-3]. During the last few years, various independent studies in the literature, employing different experimental techniques such as FT-IR spectroscopy, differential scanning calorimetry and X-ray scattering techniques showed that a three-phase model is more appropriate to describe the structure of semicrystalline polymers [4-8]. According to this model, equation (1) is transformed to the following:

$$w_C + w_A + w_{RA} = 1 \quad (2)$$

where w_{RA} is the mass fraction of the rigid amorphous part.

*Address correspondence to this author at the Istituto di Chimica e Tecnologia dei Polimeri (CNR), Italy; Tel: +39-081-867.5059; Fax: +39-081-867.5230; E-mail: dilorenzo@ictp.cnr.it

Recent analyses revealed that the three-phase model is needed to adequately describe a number of properties of semicrystalline polymers. For poly(1-butene) it was shown that for a detailed understanding of the mechanical behavior, it is necessary to account for the role played by all the three nanophases, not by the crystal and mobile amorphous parts only. The points of coupling between the amorphous and crystalline structures, that compose the rigid amorphous part, act as nanoscopic stress-transfer, with remarkable effects on mechanical properties of the material [9]. Similarly, the rigid amorphous content needs to be explicitly taken into account to describe the yield behavior and the loss of crystallinity of poly(ethylene terephthalate) (PET) in uniaxial compression, as demonstrated in Ref. [10] upon analysis of the relation between the mechanical properties and the nanostructure of PET. The RAF is of importance also in determination of the barrier properties of semicrystalline polymers. MAF and RAF have different oxygen solubility, as quantified for PET, which mainly arises from the different specific volume of the two fractions, a property that can permit to tailor the barrier properties of PET goods [10].

Some influence of the rigid amorphous fraction on polymer melting behavior has been suggested in the literature. For poly(phenylene oxide) it was shown that the physical state of the rigid amorphous fraction controls the onset of melting [11]. The small endotherm that is often seen a few degrees above the isothermal crystallization temperature was proven to contain contributions due to mobilization of the RAF for several semicrystalline polymers, like nylon 6, isotactic polystyrene and many others [12-17]. For poly(ethylene terephthalate) it was demonstrated that this small endotherm arises from devitrification of the RAF and partial melting, and that the two processes take place simultaneously, being largely coupled [16-17]. For *cis*-PBD we have recently shown that not only the first endotherm, as seen for other semicrystalline polymers, but the overall multiple melting behavior is affected by the physical state of the RAF [18].

1874-3439/10

The above discussion points to the importance of quantitative description of semicrystalline polymers in terms of the three-phase structure, for a proper understanding of materials properties. The three-phase structure may be affected by specific features of the polymer chain, like stereoregularity or degree of branching. These features influence not only the three-phase composition, but the overall thermal properties of the material. Such a study is the topic of the present article, where an investigation of the effects of chain regularity on the thermal properties and the three-phase composition of *cis*-1,4-polybutadiene is detailed.

EXPERIMENTAL PART

Materials

cis-1,4-polybutadiene samples with different microstructure were specifically synthesized for this study using neodymium-based catalytic systems. They were kindly provided by Polimeri Europa S.p.A. (Ravenna, Italy). The molecular characteristics of the analyzed grades are given in Table **1**, which reports the weight-average (M_w) and number-average (M_n) molecular mass, the molecular mass distributions and information on linearity and degree of branching of the used materials. The various samples were identified by a notation code, shown in the first column of Table **1**, on the basis of contents of *cis* units and branching.

Differential Scanning Calorimetry

Thermal properties were measured with a Mettler DSC822^e equipped with a liquid nitrogen cooling system. The instrument was calibrated in temperature with high purity standards (indium, naphthalene and cycloexane) and in energy with heat of fusion of indium. Dry nitrogen was used as purge gas at a rate of 50 ml/min. Each measurement was repeated three times to improve accuracy.

To investigate the overall kinetics of isothermal crystallization, PBD samples were heated from room temperature to 70 °C at a rate of 20 °C/min, equilibrated at 70 °C for 3 minutes, then cooled at 30 °C/min to the desired crystallization temperature (T_c) where they were allowed to crystallize.

In order to set the structure for the analysis of melting behavior, each *cis*-PBD sample was maintained at 70 °C for 3 min, then cooled at -30 °C/min to the crystallization temperature T_c = -26 °C, where it was allowed to crystallize for 1 h. After isothermal crystallization PBD was cooled at -10 °C/min to -130 °C, equilibrated at -130 °C for 3 min, then heated until complete melting using either a constant scanning rate, of either 1 or 10 °C/min, or a modulated temperature profile.

The TMDSC program was designed using the Star^e software of Mettler-Toledo, Inc. Non-isothermal TMDSC data were gained using a sawtooth oscillation with a temperature amplitude (A_T) of 0.2 °C, an underlining heating rate (q) of 1 °C/min and modulation periods (p) of 60, 90, and 120 s. From TMDSC measurements the reversing specific heat capacity ($c_{p,rev}$) was derived from the ratio of the amplitudes of modulated heat flow rate ($A_{\Phi,n}$) and temperature ($A_{T,n}$), both approximated with Fourier series [19]:

$$c_{p,rev}(\omega,n,t)=\frac{A_{\Phi,n}(t)}{A_{T,n}(t)}\ \frac{K(\omega,n,t)}{mn\omega} \qquad (3)$$

where t is the time, n the order of the harmonic, ω the base modulation frequency ($\omega=2\pi/p$), m the mass of the sample and $K(n,\omega,t)$ the frequency-dependent calibration factor. The reversing specific heat capacity data reported in this contribution were obtained from the first harmonics of the Fourier series.

Optical Microscopy

Spherulite growth rates were estimated by optical microscopy, using a Zeiss polarizing microscope equipped with a Linkam TMHS 600 hot stage and a Linkam CS 196 unit for fast cooling with liquid nitrogen. Samples for optical microscopy analysis were prepared by casting a drop of a 2 % toluene solution onto a glass slide, followed by drying under vacuum. The radius of the growing crystals was monitored during solidification by taking photomicrographs at appropriate intervals of time, using a JVC TK-1085E Video Camera. Spherulite radii were measured with the software Image-Pro Plus 3.0. Dry nitrogen gas was purged throughout the hot stage during all measurements and thermal treatments.

The thermal treatments before isothermal crystallization were identical to those used in calorimetry, and again each measurement was repeated three times. Spherulite growth rates (G) data were obtained in isothermal conditions from the initial slope of the radius (r) vs. time (t) plots [20].

RESULTS AND DISCUSSION

Fig. (**1**) illustrates the spherulite growth rates (G) of the various materials as function of the crystallization temperature. As expected, in the analyzed temperature range the rate of crystal growth decreases with temperature. The fastest crystallization rate is seen in the sample with linear structure, containing 98% of *cis* units. Overall, G increases with chain regularity, as faster transition rates are observed for the polymers that have higher stereospecificity. The introduction of units with different configuration leads to slower phase

Table 1. Molecular Characteristics of the *cis*-1,4-Polybutadiene Grades Used

Code	cis %	Mw (kDa)	Mn (kDa)	Mw/Mn	Structure
98-li	98	437	148	2.95	Linear
97-sb	97	380	100	3.8	Slightly branched
95-al	95	326	136	2.4	Almost linear
94-sb	94	360	144	2.5	Slightly branched
93-hb	93	354	136	2.6	Highly branched

transition kinetics. For the analyzed compositions, the influence of chain linearity is also of importance, as very low rates of crystal growth are measured for the branched *cis*-PBD polymers containing less than 94 % of repeating segments in the *cis* configuration.

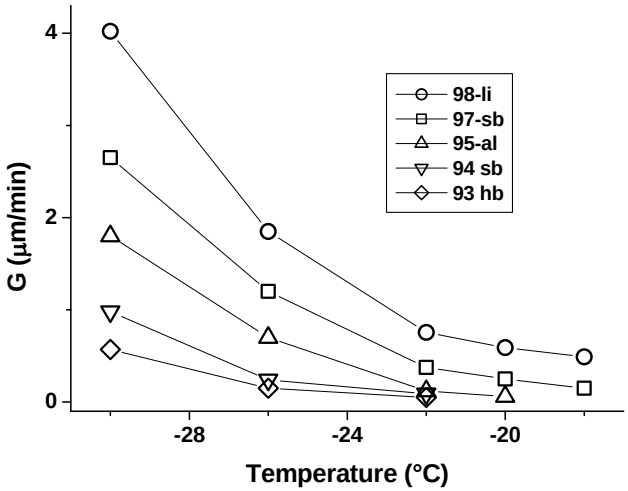

Fig. (1). Spherulite growth rate of *cis*-PBD as a function of temperature.

The overall crystallization rate of cis-PBD is presented in Fig. (**2**), that reports the data of half-time of crystallization ($\tau_{1/2}$) as a function of temperature. Fig. (**2**) reveals that relatively fast crystallization rate is attained by the commercial grade containing 97 % of *cis* segments, and that no specific trend can be correlated with chain structure, as for all the other compositions the $\tau_{1/2}$ values are very similar, close to the experimental error. Even the significant polydispersity of the various grades, that may result in segregation effects [21], has no significant influence on crystallization rate.

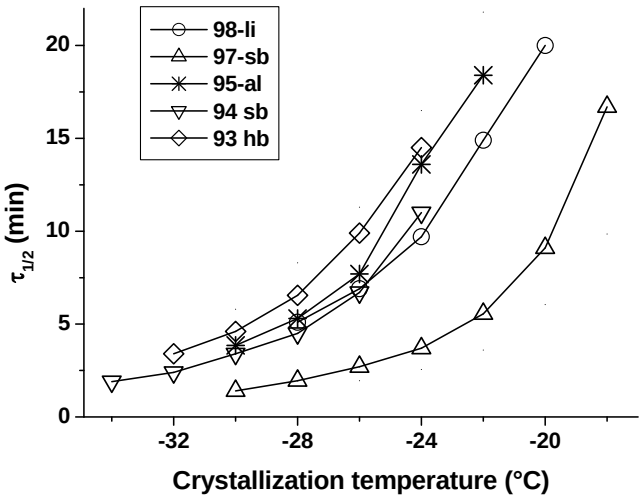

Fig. (2). Half-time of crystallization of cis-PBD as a function of temperature.

The data reported in Figs. (**1**-**2**) indicate a main influence of primary nucleation on crystallization kinetics of the analyzed *cis*-PBD grades. The overall crystallization rate is determined by superposition of the rates of crystal nucleation and growth. The process of crystallization of polymers from the melt starts with primary nucleation, then continues with crystal growth and secondary crystallization [21]. As demonstrated in Ref. [22], the analyzed *cis*-PBD grades contain different types and/or amounts of heterogeneities that are more or less active to initiate the phase transition, and this process predominates over the kinetics of crystal growth. Overall, this results in a lack of correlation of the overall crystallization rate with chain structure, as well as with polydispersity, seen in Fig. (**2**). The onset of phase transition is determined by the activity of the foreign particles present in each *cis*-PBD sample. These are responsible for an anticipated beginning of the transition, that then proceeds with a rate that is mostly affected by chain structure, quantified in Fig. (**1**).

As mentioned above, crystallization data are needed for a complete description of the thermal properties of the *cis*-PBD grades, being the material structure defined upon crystallization, that proceeds, for each sample, with the kinetics detailed in Figs. (**1**-**2**).

The melting behavior of *cis*-PBD is illustrated in Fig. (**3**) at two different heating rates, 1 and 10°C/min, for the linear grade with 98 % of *cis* units in the chain. Experimental specific heat capacity of 98-li *cis*-PBD, measured after isothermal crystallization at -26 °C for 1 h, followed by cooling to -130 °C, is compared in Fig. (**3**) with thermodynamic c_p values of fully solid and liquid *cis*-PBD, as taken from the ATHAS Data Bank [23]. The insert in the upper left corner of Fig. (**3**) presents an enlargements of the DSC traces of 98-li *cis*-PBD in the glass transition region. The c_p curves start to deviate from the baseline c_p data of solid polybutadiene at around -120 – -115 °C, due to the onset of the glass transition (T_g). The temperature range where T_g takes place is affected by heating rate, moving to higher temperatures with the increase of the scanning rate, as typical for devitrification [24]. Additional thermal events partly cover T_g in this temperature range, better seen in the enlargement presented as insert in Fig. (**3**), and the overall heat capacity jump appears to be affected by the experimental conditions, hindering a quantitative analysis of the amorphous fraction that mobilizes at T_g by conventional DSC. In order to separate the various reversing and non-reversing thermal events occurring in the glass transition region, temperature-modulated calorimetry analyses were conducted.

The reversing c_p plots determined from the TMDSC experiments at the underlying heating rate of 1 °C/min and various frequencies of modulation are compared in Fig. (**4**) with the conventional DSC traces reported in Fig. (**3**). Below the glass transition region and above completion of melting, DSC and TMDSC experimental data well agree with thermodynamic c_p of solid and liquid PBD, respectively. In the melting range the DSC and TMDSC signals are comparable. Erroneous deconvolution of the modulated signal occurs frequently when transitions with high latent heats are analyzed in TMDSC with an underlying heating rate. If irreversible endotherms and exotherms overlap, as is often the case in the analysis of the melting of polymers, the reversing heat capacities may even give larger contributions than the total latent heat, as demonstrated in Ref. [25-26]. In the temperature region of T_g, a minor frequency-dependence of the reversing heat capacity can be observed. The transition ob-

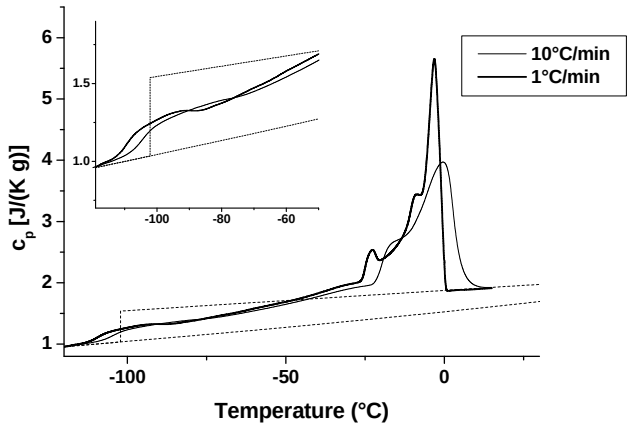

Fig. (3). Experimental specific heat capacity of 98-li *cis*-PBD measured upon heating by conventional DSC at the indicated rates, after isothermal crystallization at -26 °C for 1 h and subsequent cooling to -130 °C. The specific heat capacity of the solid and liquid *cis*-PBD, shown as dashed lines, are taken from the ATHAS data bank [23]. The insert in the upper left corner is an enlargement of the plot in the glass transition area.

tained from the reversing c_p curves of the temperature-modulated data (dynamic T_g), is located at temperatures slightly higher than the thermal glass transition measured under linear heating. This discrepancy is caused by the differences in the frequencies of the TMDSC analyses with those related to the ordinary linear heating rates, the latter being generally lower [27-29]. At completion of T_g, the reversing c_p curves gained by non-isothermal TMDSC data at three different frequencies overlap, revealing the real extent of the transition, apart from non-reversing events that inhibit correct determination of glass transition parameters of *cis*-PBD by conventional DSC. The heat capacity jump determined from the reversing c_p plots accounts for a mobile amorphous content w_A of 0.41_3.

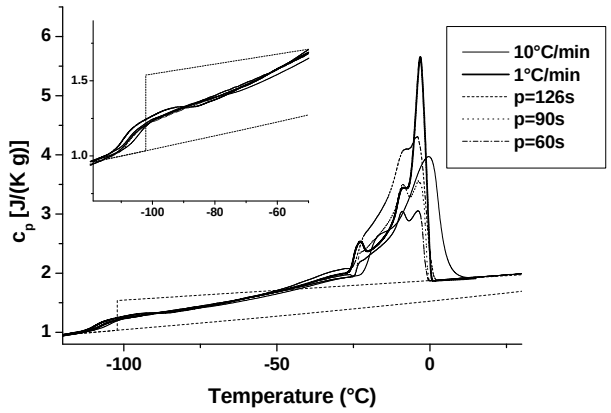

Fig. (4). Specific heat capacity of 98-li *cis*-PBD after isothermal crystallization at -26 °C and subsequent cooling, as measured upon heating. The solid lines are the total heat capacity by conventional DSC at the indicated rates, the thin lines are the reversing specific heat capacity measured by TMDSC at 1 °C/min and at the indicated periods of modulation. The specific heat capacity of the solid and liquid *cis*-PBD, shown as dashed lines, are taken from the ATHAS data bank [23].

The thermal properties of a number of grades of *cis*-PBD are shown in Fig. (**5**), that reports the DSC traces after isothermal crystallization at -26°C for 1 h followed by cooling to -130 °C. The DSC plots presented in Fig. (**5**) refer to a heating rate of 1 °C/min, which was selected for being low enough to permit a good separation of the multiple thermal events occurring in the melting region, as seen by comparison of the St-DSC traces of the 98-li polymer in Fig. (**3**), and at the same time sufficiently high to allow a good signal-to-noise ratio. The various thermograms display a glass transition centered around -108 °C overlapped by additional thermal events of endothermic nature, discussed above, and a complex melting behavior.

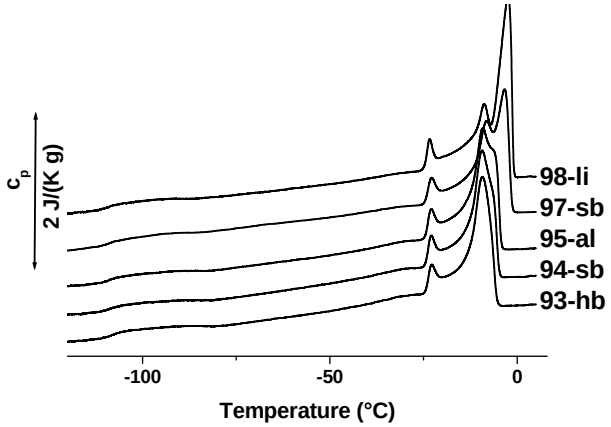

Fig. (5). Specific heat capacity of the various *cis*-PBD after isothermal crystallization at -26 °C and subsequent cooling, as measured during heating at 1 °C/min.

As probed in Figs. (**3-4**) for the 98-li grade, analysis by St-DSC does not permit to measure the heat capacity step at the glass transition, necessary to quantify the content of mobile amorphous phase of PBD, which can instead be accomplished by temperature-modulated calorimetry. A comparison of the reversing specific heat capacity of the discussed *cis*-PBD polymers, measured by TMDSC at the same period of modulation of p = 120 s, is illustrated in Fig. (**6**). The reversing c_p curves of the various samples mostly overlap from below the T_g of the MAF up to about -80 °C, with some slight differences seen only in the breadth of the glass transition event, then display large dissimilarities in the reversing melting behavior, which however is not quantitative when analyzed by TMDSC with a non-zero underlying heating rate. Most importantly, the reversing c_p curves evidence that the mobile amorphous fraction does not vary, within the experimental uncertainty, for the analyzed *cis*-PBDs after isothermal crystallization at -26°C for 1 h.

The crystal fraction is quantified by integration of St-DSC plots, using eq. (4) [30-31]:

$$c_p(T) = w_C(T)c_{p,C}(T) + w_A(T)c_{p,A}(T) - \left[h_A(T) - h_C(T)\right]\frac{dw_C(T)}{dT} \qquad (4)$$

where $c_p(T)$ is the measured specific heat capacity, $c_{p,C}(T)$ and $c_{p,A}(T)$ the thermodynamic values of the crystalline and mobile amorphous specific heat capacities and $[h_A(T)\text{-}h_C(T)]$ the heat of fusion, all tabulated in the ATHAS Data Bank [6]. Results of this analysis are presented in Fig. (**7**), that illustrates the evolution of crystal fraction with temperature

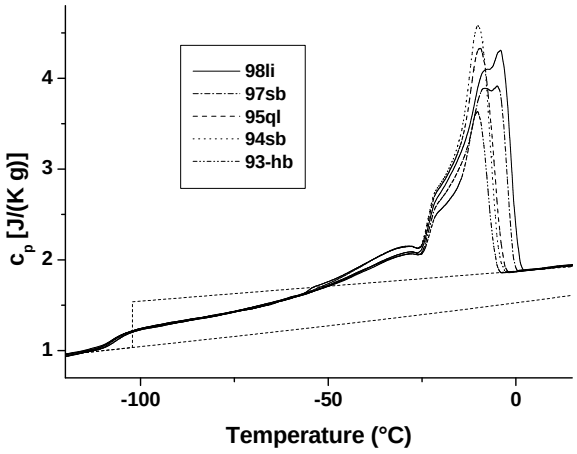

Fig. (6). Specific heat capacity of the various *cis*-PBD after isothermal crystallization at -26 °C and subsequent cooling, as measured during modulated heating at 1 °C/min and p = 120 s.

during fusion of the various PBD grades. As suggested in Ref. [32-33], the initial crystalline weight fraction of the material can be approximated by the maximum in the w_C vs. temperature plot. The crystallinity values deduced from the data of Fig. (**7**) are reported in Table **2**. Comparison with the amount of mobile amorphous phase quantified by the heat capacity step at the glass transition probes that a considerable rigid amorphous fraction (w_{RA}) develops in the *cis*-1,4-polybutadienes under the experimental conditions, which is also reported in Table **2**. It needs to be underlined that the w_{RA} values of Table **2** are probably underestimated, due to the approximation in calculation of the crystal fraction of eq. (4), that neglects possible devitrification of the RAF in the melting range. No information on the kinetics of RAF devitrification can be provided by analysis of the reversing c_p plots shown in Fig. (**3**), that display a clear frequency-dependence starting from about -80°C, when reversing and non-reversing latent heat exchanges overlap possible initial mobilization of the rigid amorphous fraction.

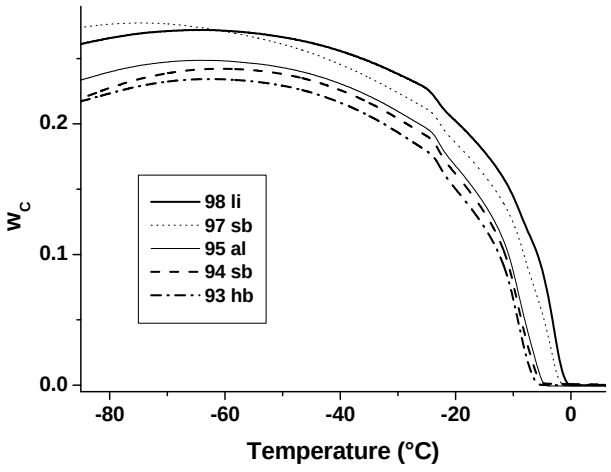

Fig. (7). Temperature dependence of the enthalpy-based crystallinity of *cis*-PBD during heating at 1 °C/min, calculated with eq.(4).

Table 2. Nanophases' Content of the *cis*-1,4-Polybutadiene Grades Used after Isothermal Crystallization at -26 °C for 1 h Followed by Cooling to -130 °C

Code	w_A	w_C	w_{AR}
98-li	0.41_3	0.27_2	0.31_5
97-sb	0.41_3	0.27_7	0.31_0
95-al	0.41_3	0.24_9	0.33_8
94-sb	0.41_3	0.24_2	0.34_5
93-hb	0.41_3	0.23_5	0.35_2

The data shown in Table **2** reveal that no straightforward relation between chain microstructure and nanophase content can be derived for *cis*-PBD, as the effects of crystallization kinetics overlap with chain regularity. For a same thermal history (isothermal crystallization at -26 °C for 1 h followed by cooling to -130 °C), the analyzed polymers develop the same amount of mobile amorphous fraction. Crystallinity roughly increases with chain regularity, as the grades with a low *cis* fraction display low levels of crystallinity. Crystallization rate also affects composition of the 3-phase structure, since the 97-sb grade, that has the fastest transition kinetics, probably due to the presence of nucleating agents in the formulations, is the polymer that develops the largest crystal fraction. This in turn, corresponds to a low RAF. Crystallization of PBD at -26 °C is completed in 8 – 25 min, depending on the grade. The time of residence at -26 °C was extended for all the samples to 1 h, in order to provide exactly the same thermal treatment for all the polymers. This corresponds to a longer time available for crystal perfection following primary crystallization to the grades that crystallize faster. The structural rearrangements following primary crystallization allow development of a larger crystal fraction, which in turn results in a reduction of the strained amorphous portions coupled with the perfected material. It is interesting to note that this process involves only the crystal-rigid amorphous interface, with no influence of the bulk amorphous phase that attains the same level in all the analyzed polymers.

As mentioned above, the multiple melting behavior of cis-PBD is illustrated in Fig. (**5**). All the analyzed grades display a small endotherm centered at -23°C, i.e. 3°C above the temperature of isothermal crystallization. This small DSC peak, that appears in a number of semicrystalline polymers a few degrees above the crystallization temperature, arises from the simultaneous occurrence of partial fusion of the crystals and enthalpy recovery connected to structural relaxation of part of the rigid amorphous fraction, as also discussed in the Introduction Section [16-17]. Neither the specific chain regularity, nor the three-phase composition seem to affect this small thermal event, at least for the analyzed *cis*-PBD grades. Conversely, large differences in the major melting peaks are displayed by the various samples. The PBD grades with a large content of *cis* units have melting endotherms centered at -9 and -3 °C. When *cis* content decreases below 95 %, the two endotherms merge in a single peak, with a small shoulder appearing in the high temperature side of the peak in the samples with 94 and 95% *cis*

segments. No shoulder is instead detectable in the major melting peak of the 93-hb *cis*-PBD grade, which has not only the smallest *cis* units percentage in the chain, but also a highly branched structure. This specific polymer has also a low crystallization rate, as quantified in Figs. (**1** and **2**).

In Ref. [18] it was shown that devitrification of the rigid amorphous fraction overlaps fusion in *cis*-PBD. Not only the first endotherm, as seen for other semicrystalline polymers, but the overall multiple melting behavior is affected by the physical state of the RAF. The multiple endotherms seen in the DSC plots of *cis*-PBD arise from partial melting and recrystallization. Upon heating, the strained amorphous segments start to mobilize, allowing the onset of melting of the crystals that have reached the upper limit of their thermal stability, and can subsequently develop more stable structures. To allow development of perfected crystals with improved thermal stability in the temperature range of the second major endotherm it is necessary that rigid amorphous fraction attains sufficient mobility. Two distinct major melting peaks are seen only in the PBD grades with high *cis* content that develop considerable crystallinity, and lower degree of RAF. These two polymers also display a large crystal fraction, compared to the other samples, and the crystal fraction develops at the expense of the RAF. It is possible that the rigid amorphous fraction in the grades with 97 % and more of *cis* segments is more strained than in the other PBD polymers, and the high degree of coupling between the rigid amorphous fraction and the crystal phase in PBD results in multiple melting appearance of the DSC traces. However, this is just a hypothesis, as the multiple melting seen in the grades with at least 97 % *cis* units may arise from the higher degree of perfection of the crystallites, together with a faster recrystallization kinetics, that facilitate partial melting followed by recrystallization into thickened and less defective crystallites during the DSC scan at 1 °C/min. Conversely, in the *cis*-PBD polymers with a less regular chain partial melting is followed by very limited recrystallization, that does not result in a separate endothermic peak, but only as a small shoulder in the DSC trace.

CONCLUSIONS

Conventional and temperature-modulated DSC analyses allowed to quantify the influence of chain microstructure on thermal properties of *cis*-PBD. All the analyzed grades develop, upon isothermal crystallization from the melt followed by cooling, a three-phase structure, whose composition depends on the specific features of the polymer chain, as well as on crystallization kinetics. All the analyzed grades have the same amount of mobile amorphous phase, whereas dissimilarities exist in crystallinity level and rigid amorphous content.

Similarly to other semicrystalline polymers, *cis*-PBD displays a small endotherm a few degrees above the isothermal crystallization temperature. This thermal event, that is caused by concurrent partial melting of the crystal phase and partial devitrification of the rigid amorphous fraction, is independent of chain structure and composition. Additional endotherms are also present at higher temperatures. The polybutadienes with a high *cis* content show two separate endothermic events at high temperatures, caused by partial melting and recrystallization, which overlap with full mobilization of the rigid amorphous fraction. In the grades with lower degree of chain regularity, the two endotherms merge into a single peak, at least under the used experimental conditions, as the partial melting-recrystallization processes take place to a more limited extent.

ACKNOWLEDGEMENTS

The author wishes to thank Dr. Eng. Fabio Montanari and Dr. Eng. Salvatore Coppola of Polimeri Europa (Ravenna, Italy) for kindly providing the polybutadiene sample, as well as Dr. Maria Cristina Righetti of IPCF-CNR for useful discussions.

REFERENCES

[1] Tate, D.P; Betea, T.W. *Butadiene Polymers*. In: *Encyclopedia of Polymer Science and Technology*, 2nd ed. Mark, H.F.; Bikales, N.M.; Overberger, C.G.; Menges, G., Eds; John Wiley and Sons: New York, **1985**.

[2] Suzuki, H.; Grebowicz, J.; Wunderlich, B.; Heat capacity of semicrystalline, linear poly(oxymethylene) and poly(oxyethylene). *Makrom. Chem*., **1985**, *186*, 1109-1119.

[3] Wunderlich, B. Reversible crystallization and the rigid–amorphous phase in semicrystalline macromolecules. *Progr. Polym. Sci*., **2003**, *28*, 383-450.

[4] Kitamaru, R.; Horii, F.; Murayama, K. Phase structure of lamellar crystalline polyethylene by solid-state high-resolution carbon-13 NMR detection of the crystalline-amorphous interphase. *Macromolecules*, **1986**, *19*, 636-643.

[5] Kunz, M.; Möller, M.; Heinrich, U.R.; Cantow, H.J. Electron spectroscopic imaging studies of polyethylene, chain-folded and extended-chain crystals. *Makromol. Chem. Macromol. Symp*., **1988**, *20/21*, 147-158. Electron spectroscopic imaging studies on semicrystalline and block-copolymer systems. *Makromol. Chem. Macromol. Symp*., **1989**, *23*, 57-72.

[6] Gabriels, W.; Gaur, H.A.; Feyen, F.C.; Weeman, W.S. ^{13}C solid-state NMR study of differently processed poly(ethylene terephthalate) yarns. *Macromolecules*, **1994**, *27*, 5811-5820.

[7] Cheng, J.; Fone, M.; Reddy, V.N.; Schwartz, K.B, Fisher HP, Wunderlich B. Identification and quantitative analysis of the intermediate phase in a linear high-density polyethylene. *J. Polym. Sci*.: *Part B*: *Polym. Phys*., **1994**, *32*, 2683-2693.

[8] Litvinov, V.M.; Mathot, V.B.F. Partitioning of main and side-chain units between different phases: A solid-state ^{13}C NMR inversion-recovery cross-polarization study on a homogeneous, metallocene-based, ethylene-1-octene copolymer. *Solid State Magn. Reson*., **2002**, *22*, 218-234.

[9] Di Lorenzo, M.L.; Righetti, M.C. The three-phase structure of isotactic poly(1-butene). *Polymer*, **2008**, *49*, 1323-1331.

[10] Lin, J.; Shenogin, S.; Nazarenko, S. Oxygen solubility and specific volume of rigid amorphous fraction in semicrystalline poly(ethylene terephthalate). *Polymer*, **2002**, *43*, 4733-4743.

[11] Pak, J.; Pyda, M.; Wunderlich, B. Rigid amorphous fractions and glass transitions in poly(oxy-2,6-dimethyl-1,4-phenylene). *Macromolecules*, **2003**, *36*, 495-499.

[12] Xu, H.; Ince, S.; Cebe, P. Development of the crystallinity and rigid amorphous fraction in cold-crystallized isotactic polystyrene. *J. Polym. Sci. Part B*: *Polym. Phys*., **2003**, *41*, 3026-3036.

[13] Lu, S.X.; Cebe, P. Effects of annealing on the disappearance and creation of constrained amorphous phase. *Polymer*, **1996**, *37*, 4857-4863.

[14] Lee, Y.; Porter, R.S. Double-melting behavior of poly(ether ether ketone). *Macromolecules*, **1987**, *20*, 1336-1341.

[15] Cheng, S.Z.D.; Wunderlich, B. Glass transition and melting behavior of poly(ethylene 2,6-naphthalenedicarboxylate). *Macromolecules*, **1988**, *21*, 789-797.

[16] Righetti, M.C.; Di Lorenzo, M.L.; Tombari, E.; Angiuli, M. The low-temperature endotherm in poly(ethylene terephthalate): Partial melting and rigid amorphous fraction mobilization. *J. Phys. Chem. B*, **2008**, *112*, 4233-4241.

[17] Righetti, M.C.; Di Lorenzo, M.L. Vitrification and devitrification of the rigid amorphous fraction in poly(ethylene terephthalate). *e-polymers*, **2009**, n° 053.

[18] Di Lorenzo, M.L. The melting process and the rigid amorphous fraction of *cis*-1,4-polybutadiene. *Polymer*, **2009**, *50*, 578-584.
[19] Androsch, R.; Moon, I.; Kreitmeier, S.; Wunderlich, B.; Determination of heat capacity with a sawtooth-type, power-compensated temperature-modulated DSC. *Thermochim. Acta*, **2000**, *357-358*, 267-278.
[20] Di Lorenzo, M.L. Spherulite growth rates in binary polymer blends. *Progr. Polym. Sci.* **2003**, *28*, 663-689.
[21] Wunderlich, B., *Macromolecular Physics. Vol. 2: Crystal Nucleation, Growth Annealing*, Academic Press: New York, **1976**.
[22] Di Lorenzo, M.L. Crystallization kinetics of *cis*-1,4-polybutadiene. *J. Appl. Polym. Sci*., DOI 10.1002/app.30681. Published online: 4 Jan 2010.
[23] ATHAS Data Bank. Pyda M, editor. http://athas.prz.rzeszow.pl/ (accessed Feb 2009)
[24] Wunderlich B. *Thermal Analysis of Polymeric Materials*, Springer-Verlag: New York, **2005**.
[25] Di Lorenzo, M.L.; Wunderlich, B. Temperature-modulated calorimetry of the crystallization of polymers analyzed by measurements and model calculations. *J. Therm. Anal. Calor*., **1999**, *57*, 459-472.
[26] Di Lorenzo, M.L.; Wunderlich, B. Melting of polymers by non-isothermal, temperature-modulated calorimetry: analysis of various irreversible latent heat contributions to the reversing heat capacity. *Thermoch. Acta*, **2003**, *405*, 255-268.
[27] Hensel, A; Schick, C.; Relation between freezing-in due to linear cooling and the dynamic glass transition temperature by temperature-modulated DSC. *J. Non-Cryst. Solids*, **1998**, *235-237*, 510-516.
[28] Montserrat, S.; Calventus, Y.; Hutchinson, J.M. Effect of cooling rate and frequency on the calorimetric measurement of the glass transition. *Polymer*, **2005**, *46*, 12181-12189.
[29] Hutchinson, J.M.; Ruddy, M. Thermal cycling of glasses. III. Upper peaks. *J. Polym. Sci., Polym. Phys. Edn*., **1990**, *28*, 2127-2163.
[30] Mathot, V.B.F.; Scherrenberg, R.L.; Pijpers, M.F.J.; Bras, W. *J. Thermal Anal*., **1996**, *46*, 681-718.
[31] Mathot, V.B.F. in: *Calorimetry and Thermal Analysis of Polymers*, Mathot, V.B.F. Ed., Hanser/Gardner, Cincinnati, **1994**; pp. 105-167.
[32] Righetti, M.C.; Tombari, E.; Angiuli, M.; Di Lorenzo, M.L. Enthalpy-based determination of crystalline, mobile amorphous and rigid amorphous fractions in semicrystalline polymers: Poly(ethylene terephthalate). *Thermochim. Acta*, **2007**, *462*, 15-24.
[33] Righetti, M.C.; Tombari, E.; Angiuli, M.; Di Lorenzo, M.L.; Crystalline, mobile amorphous and rigid amorphous fractions in isotactic polystyrene. *Eur. Polym. J*., **2008**, *44*, 2659-2667.

Received: November 20, 2009 Revised: December 11, 2009 Accepted: December 15, 2009